A Canonical Approach to Generate Multidimensional Potential Energy Surfaces

Jay R. Walton

Department of Mathematics, Texas A&M University, College Station, Texas 77843-3368, USA

Luis A. Rivera-Rivera*

Department of Physical Sciences, Ferris State University, Big Rapids, MI 49307-2225

Robert R. Lucchese, John W. Bevan

Department of Chemistry, Texas A&M University, College Station, Texas 77843-3255, USA

Abstract

A new force-based canonical approach for the accurate generation of multidimensional potential energy surfaces is demonstrated. Canonical transformations previously developed for diatomic molecules are used to construct accurate approximations to the 3-dimensional potential energy surface of the water molecule from judiciously chosen 1-dimensional planar slices that are shown to have the same canonical shape as the classical Lennard-Jones potential curve. Spline interpolation is then used to piece together the 1-dimensional canonical potential curves, to obtain the full 3-dimensional potential energy surface of water molecule with a relative error less than 0.01. This work provides an approach to greatly reduce the computational cost of constructing potential energy surfaces in molecules from *ab initio* calculations. The canonical transformation techniques develop in this work illuminate a pathway to deepening our understanding of chemical bonding.

* To whom correspondence should be addressed. E-mail: LuisRiveraRivera@ferris.edu

I. Introduction

The concept of the Born-Oppenheimer potential energy surface (PES) has been and continues to be of central importance for understanding, characterizing, and predicting properties associated with molecular structure, spectroscopy, and reaction dynamics.[1-5] With advances on computer power and increasing efficacy of *ab initio* methods, it is now possible to calculate *ab initio* points on the PES with high accuracy, and in most cases within chemical accuracy (1 kcal/mol). However, it still computationally costly to generate a reliable PES from calculated *ab initio* points for systems that have more than 4 atoms. The challenge lies on the generation of an accurate global representation of a multidimensional PES with a minimum number of calculated *ab initio* points.

Different approaches have been proposed to generate multidimensional PES from *ab initio* points.[6-14] In general, these approaches can be classified as interpolation methods that ensure that the PES reproduces all *ab initio* points, or as fitting methods where the *ab initio* points are fit to a multidimensional analytical function. Global interpolations methods are in general of high accuracy if an adequate number of *ab initio* points are used, however, they are computationally prohibited for systems of high dimensions. In contrast, fitting methods are computationally less expensive and are the normal choice for systems of high dimensions. PES generated by fitting approaches do not reproduce the *ab initio* points, but strive to minimize the global error of the fitting involving a large number of adjustable parameters that in most cases do not have physical significance. Recently, automatic procedure of PES generation has been proposed,[15,16] aiming minimal human input and effort.

This work presents a new force-based canonical approach to generate highly accurate multidimensional PES. Canonical approaches[17-26] have been recently developed and extensively

applied to diatomic molecules and multidimensional intermolecular interactions along the dissociative coordinate. Applications of canonical approaches have led to the discovery of canonical potentials and to their application to generate highly accurate potential curves of pairwise interatomic interactions. The term canonical potential refers to dimensionless functions obtained from each molecule within the defined class by a readily invertible algebraic transformation. Furthermore, to be deemed canonical, the dimensionless potentials obtained from all of the molecules within the defined class by the canonical transformation must agree to within a specified order of high accuracy. The potential curves of pairwise interatomic interactions generated by canonical approaches do not require the use of adjustable parameter and the quality of the generated potentials are close to spectroscopy accuracy (1 cm^{-1}, 0.0028591 kcal/mol).

Furthermore, the previous adaptions of canonical approaches were then applied to algebraic forms of the classic Morse, Lennard-Jones, and Kratzer potentials.[25] Using the classic Morse, Lennard-Jones, or Kratzer potential as reference, inverse canonical transformations allow the accurate generation of Born-Oppenheimer potentials for H_2^+ ion, neutral covalently bound H_2, van der Waals bound Ar_2, and the hydrogen bonded 1-dimensional dissociative coordinate in water dimer. In addition, an algorithmic strategy based upon a canonical transformation to dimensionless form applied to the force distribution associated to a potential was developed. This algorithm lead to accurate approximations to both the force and potential functions corresponding to a particular diatomic molecule in terms of the force distribution associated with an algebraic potential energy function, such as the Lennard-Jones function. Now, this methodology is extended and apply to the 3-dimensional water molecule PES. The 3-dimensional PES of the water molecule is accurately constructed from judiciously chosen 1-dimensional planar slices that are shown to have the same canonical shape as the classical

Lennard-Jones potential curve. The highly accurate water potential of Polyansky *et al*.[27] was used to generate the necessary data for the analysis presented in this work.

II. Methods

As illustrated in Figure 1, the PES for H_2O can be viewed as a 3-dimensional surface imbedded in 4-dimensional Euclidean space that can be viewed as the graph of real-valued function of three variables. The three degrees of freedom shown in Figure 1 are Θ, the H-O-H bond angle, R_1 and R_2, the two O-H bond lengths. The H_2O PES can be constructed as a graph in 4-dimensional space of a potential function of Θ, R_1 and R_2 with $0 \leq \Theta \leq 180$ (in degrees), and $0 < R_1, R_2 < \infty$. Planar slices of this PES give 1-dimensional potential curves. One judiciously chosen family of such planar slices, produces 1-dimensional potential curves that have the same canonical shape arising in diatomic molecules as studied previously.[17-26] To define this judicious family of planar slices, it is convenient to introduce polar coordinates in the (R_1, R_2)-quarter-plane spanned by $0 < R_1, R_2 < \infty$. Defining $\Phi = \arctan(R_2/R_1)$ and $R = \sqrt{R_1^2 + R_2^2}$, one can view the full H_2O PES as the graph of a function $E(R,\Theta,\Phi)$. Appealing to obvious symmetries, one can restrict attention to $E(R,\Theta,\Phi)$ with $0 < R$, $0 < \Theta < 180$ degrees, $0 < \Phi < 45$ degrees. The desired planar slices are defined by fixing values for both Φ and Θ. It should be noted in Figure 1 that this corresponds to fixing the bond angle Θ and fixing the ratio R_2/R_1. These planar slices yield a family of 1-dimensional curves $E(R;\Theta,\Phi)$, $0 < R < \infty$ with Φ and Θ held constant. Figure 2 shows examples of these planar slices for $\Theta = 94°$. While these curves appear to be rather different for the five different values of Φ, they do in fact have the same canonical shape as the diatomic molecules considered in Refs. 17–26 and as the classical Morse and Lennard-Jones potential curves.[25] One way to understand the canonical shapes of these curves is to view

each of these slices with Φ and Θ constant as behaving like diatomic complexes with the two hydrogen atoms held in a fixed rigid orientation ($R_2/R_1 =$ constant in a coordinate system having the oxygen atom at the origin) as they move toward or away from the oxygen atom.

Consider a generic potential slice, denoted $E(R)$, with R_2/R_1 held constant and $R^2 = R_1^2 + R_2^2$. As illustrated in Figure 2, $E(R)$ possesses a unique minimum, denoted $-D_e$, representing a dissociation energy associated with this particular potential slice. Denote by R_e the separation distance at which $E(R_e) = -D_e$. A sequence of R_j values is defined by $F(R_j) = -F_m/2^j$, for $j = 0, 1, 2, ...$, where F_m, the maximum value of the attractive force, that is, $F(R_0) = -F_m$. In particular, R_0 (also called R_m) is the internuclear separation at which the attractive force is equal to $-F_m$. Using the Lennard-Jones potential curve

$$E_{LJ}(R) = D_e\left(\left(\frac{R_e}{R}\right)^{12} - 2\left(\frac{R_e}{R}\right)^{6}\right) \tag{1}$$

as a reference potential the generic $E(R;\Theta,\Phi)$ potential curves can be approximate by using the inverse canonical transformation as

$$E(R;\Theta,\Phi) = E\left(R_j\right) + \left(E\left(R_{j+1}\right) - E\left(R_j\right)\right)\left(\frac{E_{LJ}\left(R_j^{LJ} + x\left(R_{j+1}^{LJ} - R_j^{LJ}\right)\right) - E_{LJ}\left(R_j^{LJ}\right)}{E_{LJ}\left(R_{j+1}^{LJ}\right) - E_{LJ}\left(R_j^{LJ}\right)}\right) \tag{2}$$

for $0 \le x \le 1$ defined by:

$$x = \frac{R - R_j}{R_{j+1} - R_j}. \tag{3}$$

Eq. (2) is defined for the attractive side of the potential curve, that is, $R > R_e$. The R_j^{LJ} values for the reference potential, $E_{LJ}(R)$, are defined in similar fashion as those for the target potential, $F_{LJ}\left(R_j^{LJ}\right) = -F_m^{LJ}/2^j$. Similar constructions can be carried out on the repulsive side of the potential, that is, $0 < R \le R_e$, only now one defines the sequence of $R_{rj} < R_e$, j=1,2,..., values by $F(R_{rj}) = F_m 2^j$ (and similarly for the reference potential). In particular, R_{r0} is the internuclear

separation at which the repulsive force has magnitude equal to F_m, the maximum value of the attractive force. At successive values of R_{rj}, the repulsive force doubles.

In summary, the canonical nature of the curves $E(R;\Theta,\Phi)$ for fixed values of Θ and Φ enables one to construct simple algebraic forms given by Eq. (2) for each potential slice provided one has good "estimates" for a finite number of R_j values and associated energies $E_j=E(R_j;\Theta,\Phi)$. To fix notation and to emphasize that both R_j and E_j depend upon a particular PES slice defined by fixing both Θ and Φ, we denote: $R_j=R_j(\Theta,\Phi)$ and $E_j=E_j(\Theta,\Phi)$.

Clearly, one cannot obtain the necessary data to apply the inverse canonical transform Eq. (2) to every PES slice $E(R;\Theta,\Phi)$ for $0 < \Theta < 180$ degrees, $0 < \Phi < 45$ degrees. In the next section, we discuss two strategies for obtaining good approximations to all of the desired PES slices from a finite number of such slices. The first uses direct spline interpolation from a given finite set of angle pairs $\{\Theta_i, \Phi_k, i=1,...,m \text{ and } k=1,...,n\}$ while the second makes use of a judiciously chosen canonical transformation of both $R_j(\Theta,\Phi)$ and $E_j(\Theta,\Phi)$.

III. Results

We divide the results into two subjections in which the spline interpolation and canonical transformation strategies for approximating the functions $R_j(\Theta,\Phi)$ and $E_j(\Theta,\Phi)$ from a finite set of data mentioned above are discussed separately. In both cases, the accuracy of the two different approximations is judged against values of $E(R,\Theta,\Phi)$ obtained from Polyansky *et al*. [27], which for purposes of this study are considered to be "true". However, it is important to keep in mind that most of the range of values (R,Θ,Φ) needed for the calculations performed in this paper are well into the range of values obtained via extrapolation from *ab initio* results, since these were

calculated for a rather restricted range of energies considerably lower than we used. We shall return to this crucial point when discussing results.

III.A. Direct Spline Interpolation Method

A direct spline interpolation approach to approximating the functions $R_j(\Theta,\Phi)$ and $E_j(\Theta,\Phi)$ can be implemented by selecting a finite number of values for both Θ and Φ. The theoretical bounds on Θ and Φ are: $0 < \Theta < 180$ degrees, $0 < \Phi < 45$ degrees. To test the direct interpolation method, we chose the sets of values: $\{\Theta_i, i=1,...,10\} = \{44, 64, 84, 94, 104, 114, 124, 144, 164, \text{and } 180 \text{ degrees}\}$ for Θ and $\{\Phi_k, k=1,...,9\} = \{5, 10, 15, 20, 25, 30, 35, 40, \text{and } 45 \text{ degrees}\}$ for Φ. Thus, there are 90 pairs of values $\{(\Theta_i,\Phi_k), i=1,...,10, k=1,...9\}$. For each of the 90 pairs, we computed values for $R_j(\Theta_i,\Phi_k)$ and associated energies $E_j(\Theta_i,\Phi_k)$ from the PES in Polyansky *et al*. [27]. More specifically, we chose the set of R-values: $\{R_{r6}(\Theta_i,\Phi_k), R_{r5}(\Theta_i,\Phi_k), R_{r4}(\Theta_i,\Phi_k), R_{r3}(\Theta_i,\Phi_k), R_{r2}(\Theta_i,\Phi_k), R_{r1}(\Theta_i,\Phi_k), R_{rm}(\Theta_i,\Phi_k), R_e(\Theta_i,\Phi_k), R_m(\Theta_i,\Phi_k), R_1(\Theta_i,\Phi_k), R_2(\Theta_i,\Phi_k), R_3(\Theta_i,\Phi_k), R_4(\Theta_i,\Phi_k), \text{and } R_5(\Theta_i,\Phi_k)\}$. Bivariate spline approximations were then constructed for each of these functions. Thus, for example, from the set of values: $\{(\Theta_i,\Phi_k, R_e(\Theta_i,\Phi_k)), i=1,...,10, k=1,...,9\}$ one performs standard bivariate spline interpolation to produce an approximation $\hat{R}_e(\Theta,\Phi)$ to the function $R_e(\Theta,\Phi)$. This procedure is repeated for each R_j–value and for each associated energy E_j. These interpolated functions are then substituted into the inverse canonical transformation Eq. (2) to obtain an approximation $\hat{E}(R,\Theta,\Phi)$ to the full PES $E(R,\Theta,\Phi)$ which was then compared against the "true" PES in Polyansky *et al*.[27].

To test the effectiveness of this procedure, the approximate functions $\hat{R}_j(\Theta,\Phi)$, $\hat{E}_j(\Theta,\Phi)$, and $\hat{E}(R,\Theta,\Phi)$ were compared to the true functions obtained from Polyansky *et al*.[27] for (Θ,Φ) not occurring among the "training" data $\{(\Theta_i, \Phi_k, R_e(\Theta_i,\Phi_k)), i=1,...,10, k=1,...,9\}$. As a typical

example, consider $(\Theta,\Phi) = (100°,40°)$. The goodness-of-fit measure chosen was relative error define by:

$$\frac{\left|\hat{R}_j(100^\circ,40^\circ)-R_j(100^\circ,40^\circ)\right|}{R_j(100^\circ,40^\circ)} \text{ and } \frac{\left|\hat{E}_j(100^\circ,40^\circ)-E_j(100^\circ,40^\circ)\right|}{E_j(100^\circ,40^\circ)} \tag{4}$$

for $\hat{R}_j(100^\circ, 40^\circ)$ and $\hat{E}_j(100^\circ, 40^\circ)$, and by:

$$\frac{\int_{R_{r6}}^{R_5}\left|\hat{E}(R,100^\circ,40^\circ)-E(R,100^\circ,40^\circ)\right|dR}{\int_{R_{r6}}^{R_5}\left|E(R,100^\circ,40^\circ)\right|dR} \tag{5}$$

for $\hat{E}(R, 100°, 40°)$. The computed relative errors are listed in Table 1. The left-hand graph in Figure 4 shows the true energy $E(R, 100°, 40°)$ vs. the approximation $\hat{E}(R, 100°, 40°)$. The relative error for $\hat{E}(R, 100°, 40°)$, defined by Eq. (5), was computed to be 1.9×10^{-3}.

The accuracy of the direct interpolation method clearly depends upon the "training" data, that is, the number and distribution of angle pairs $\{(\Theta_i,\Phi_k)$, i=1,...,m, k=1,...n$\}$ and associated values of $\hat{R}_j(\Theta_i,\Phi_k)$ and $\hat{E}_j(\Theta_i,\Phi_k)$; a higher density of angle pairs leads to increased accuracy. The cost of increased accuracy through a higher density of angle pairs is the increased number of *ab initio* calculations through which the values $\hat{R}_j(\Theta_i,\Phi_k)$ and $\hat{E}_j(\Theta_i,\Phi_k)$ are computed. In the next subsection, we demonstrate how making use of a certain canonical transformation of the functions $\hat{R}_j(\Theta,\Phi)$ can greatly reduce the required number of *ab initio* computations with little sacrifice of accuracy.

III.B. Canonical Transformation Method

Plotting the surfaces $\hat{R}_j(\Theta,\Phi)$ suggests that they have similar "shapes" for different values of *j*. This notion of similar shape can be made rigorous by rescaling. In particular, for each value of *j*, we define a rescaled version of $\hat{R}_j(\Theta,\Phi)$, denoted $\breve{R}_j(x, y)$ for $0 < x, y < 1$, by:

$$\breve{R}_j(x,y) = \frac{\left(R_j(180x+44(1-x),45y+5(1-y))-R_j(180x+44(1-x),5)\right)}{\left(R_j(180x+44(1-x),45)-R_j(180x+44(1-x),5)\right)} \tag{6}$$

which is readily inverted to give:

$$\hat{R}_j(\Theta,\Phi) = \hat{R}_j(\Theta,5) + \check{R}_j(x,y)\left(\hat{R}_j(\Theta,45) - \hat{R}_j(\Theta,5)\right) \tag{7}$$

with $\Theta = 180x + 44(1-x)$ and $\Phi = 45y + 5(1-y)$, or equivalently:

$$x = \frac{(\Theta-44)}{136} \text{ and } y = \frac{(\Phi-5)}{40} \tag{8}$$

Figure 3 compares the scaled functions $\check{R}_j(x,y)$ for two values of *x* and two values of *j*. One also observes that for fixed *y*, the functions $\check{R}_j(x,y)$ are nearly constant for $0 < x < 1$. Table 2 gives the relative errors between $\check{R}_{\mathrm{Re}}(x,y)$ and $\check{R}_j(x,y)$ for a range of other values of *j* where the relative error is defined by:

$$\text{Rel Err} = \frac{\int_0^1\int_0^1 \left|\check{R}_{\mathrm{Re}}(x,y) - \check{R}_j(x,y)\right| dxdy}{\int_0^1\int_0^1 \left|\check{R}_{\mathrm{Re}}(x,y)\right| dxdy}. \tag{9}$$

Appealing to Eq. (7) and the relatively small errors in Table 2 and, in particularly, the relative insensitivity of $\check{R}_{\mathrm{Re}}(x,y)$ to variations in *x*, we define the approximate forms $\tilde{R}_j(\Theta,\Phi)$ by:

$$\tilde{R}_j(\Theta,\Phi) = \hat{R}_j(\Theta,5) + \check{R}_{\mathrm{Re}}(0.5,y)\left(\hat{R}_j(\Theta,45) - \hat{R}_j(\Theta,5)\right) \tag{10}$$

with *x* and *y* defined in Eq. (8). Additionally, one defines the associated energies:

$$\tilde{E}_j(\Theta,\Phi) = \hat{E}\left(\tilde{R}_j(\Theta,\Phi)\right) \tag{11}$$

and then an approximation, denoted $\tilde{E}(R,\Theta,\Phi)$ to $E(R,\Theta,\Phi)$ obtained by substitution of $\tilde{E}_j(\Theta,\Phi)$ and $\tilde{R}_j(\Theta,\Phi)$ into Eq. (2). The right-hand graph in Figure 4 shows the true energy $E(R,100°,40°)$ vs. the approximation $\tilde{E}(R,100°,40°)$. The relative error between $E(R,100°,40°)$ and $\tilde{E}(R,100°,40°)$ was computed to be 7.9×10^{-3}. While not as good a fit as was obtained from the direct interpolation method, it is still quite good and requires much less computation to obtain the required input data.

IV. Discussion

A key factor to consider in assessing the value of a proposed strategy for constructing a PES approximation is its computational complexity by which we mean to computational effort required to implement it. As stated in the introduction to this paper, we take the PES constructed by Polyansky *et al*.[27] to be the "true" PES against which our approximation is compared. It is helpful to briefly review the strategy employed by Polyansky *et al*. and estimate its computational cost. As stated in Polyansky et al[27], they adopt the standard approach of using Radau coordinates to calculate the nuclear motion on the H_2O PES. They perform calculations using 25 DVR grid points for each radial variable and 40 angular DVR grid points. Moreover, their calculated *ab initio* points on the PES are restricted to energies below 25,000.0 cm^{-1}. For energies beyond 25,000.0 cm^{-1}, Polyansky *et al*. perform a customary extrapolation to a chosen functional form with a large number of fitting parameters, 246 in this particular case. The adjustable parameters were fit to 1260 *ab initio* points below 25,000.0 cm^{-1}.

In contrast, the procedures employed here require no adjustable parameters; all necessary parameter values are computed by explicit formulas appearing in the theory. Moreover, the PES formulas utilized here are valid for energies well beyond 25,000.0 cm^{-1}, without extrapolation, and require far fewer *ab initio* points than traditional approaches. These desirable properties of the PES approximation methods introduced here result from the observation that certain planar slices through the full H_2O PES produce curves with well-defined canonical shapes. The canonical nature of these advantageous PES slices is revealed readily by adopting a coordinate system (R,Θ,Φ) with Θ denoting the angle between the two HO bonds and (R,Φ) denoting the polar coordinate system for the (R_1,R_2) Cartesian plane of the two HO bond lengths. The first observation is that the radial slices of the full H_2O PES corresponding to fixing the two angular

variables (Θ,Φ) possess the same canonical shape seen in the wide array of diatomic molecules studied in Refs. 17–26. The direct interpolation method described above (Section III.A) exploits the canonical nature of these radial slices to construct an approximation of the full H_2O PES (for $44° < \Theta < 180°$ and $5° < \Phi < 45°$) that utilizes nine values for Φ and ten values for Θ along with fourteen of the special radial values defined by the associated (radial) force. The total number of *ab initio* points needed to calculate all of the parameters used in this PES approximation is 9×10×14 = 1260 points. However, it must be emphasized that this produces a PES approximation for energies up to 9.0×10^5 cm^{-1}. If attention is restricted to energies below 25,000.0 cm^{-1}, the number of required *ab initio* points is much reduced as gleaned from Figure 5 containing plots of the energy surfaces $E_j(\Theta,\Phi)=E(R_j(\Theta,\Phi),\Theta,\Phi)$ for various values of *j.* In particular, Figure 5a shows the set of angular variables (Θ,Φ) for which the energy surface $E_e(\Theta,\Phi)=E(R_e(\Theta,\Phi),\Theta,\Phi)$ lies below 25,000.0 cm^{-1}, while Figure 5b shows the set of angular variables (Θ,Φ) for which the energy surface $E_m(\Theta,\Phi)=E(R_m(\Theta,\Phi),\Theta,\Phi)$ lies below 25,000.0 cm^{-1}. Figure 5c shows that the entire energy surface $E_1(\Theta,\Phi)=E(R_1(\Theta,\Phi),\Theta,\Phi)$ lies above 25,000.0 cm^{-1}. Figures 5d, 5e, and 5f show on the repulsive side of radial PES slices, one need only consider the two values R_{rm} and R_{r1}. Thus, restricting to energies below 25,000.0 cm^{-1}, one need use only the four radial values $\{R_{r1}, R_{rm}, R_e, R_m\}$. It also follows from Figure 5 that restricting energies to below 25,000.0 cm^{-1} means that only four values of Φ {45, 40, 35, and 30 degrees} are required. Thus, only 126 *ab initio* points suffice to approximate the H_2O PES for energies below 25,000.0 cm^{-1}.

The second method for approximating the H_2O PES described above (Section III.B) exploits an additional canonical transformation to that applied to radial PES slices in the first method. In particular, it was shown that the planar PES slices defined by fixing R_j and Θ have a canonical

dimensionless shape. Moreover, these canonical curves (to high accuracy) are constant with respect to Θ. It follows that exploiting both this canonical shape behavior plus that for radial PES slices allows one to approximate the full H_2O PES (up to energies on the order of 9.0×10^5 cm^{-1}) using only 149 *ab initio* points to evaluate all of the required parameter values. For energies below 25,000.0 cm^{-1}, only 49 *ab initio* points are required.

Besides providing an approach to greatly reducing the computational cost of constructing PESs in molecules from *ab initio* calculations, the canonical transformation techniques utilized here illuminate a pathway to deepening our understanding of chemical bonding. This aspect of the canonical transformation methodology was recently extensively explored in the setting of diatomic molecules (see Refs. 17–26). In particular, it was shown that through consideration of force (through which the key radial separation distances R_j are defined) rather than just potential energy the canonical structure of diatomic potential curves is revealed. In the present work, a strategy for generalizing the diatomic canonical transformation paradigm to triatomic molecules via judiciously chosen planar slicing of the higher dimensional PES was proposed and exploited. As with the diatomic theory studied in Refs. 17–26, this approach to extending the canonical transformation method to triatomic molecules offers the potential to deepen our understanding of chemical bonding in larger molecules.

V. Conclusions

A canonical transformation perspective upon understanding unifying structural properties of potential energy curves for diatomic molecules was generalized to the triatomic molecule H_2O. A practical application of the resulting canonical transformation decomposition of the H_2O PES was to the development of an algorithm for constructing accurate approximations to the PES

with no adjustable fitting parameters and requiring one to two orders of magnitude fewer *ab initio* data points than traditional PES approximation methods. A key issue to explore concerning extension of this approach to other triatomic (and possibly larger) molecules is how the results obtained for the symmetric H_2O molecule depend upon that symmetrical structure. For example, would similar results obtain for triatomic molecules comprised of three different atoms? These and other questions will be studied in future investigations.

Acknowledgments

We give special thanks to the Laboratory for Molecular Simulation, the High Performance Research Computing, and the Institute for Applied Mathematics and Computational Science at Texas A&M University.

Table 1. Computed relative errors as defined by Eq. (4).

	$\hat{R}_j(100°,40°)$	$\hat{E}_j(100°,40°)$
R_{r6}	2.5×10^{-4}	7.3×10^{-4}
R_{r5}	9.9×10^{-5}	2.3×10^{-4}
R_{r4}	1.2×10^{-5}	6.7×10^{-4}
R_{r3}	7.5×10^{-5}	1.0×10^{-3}
R_{r2}	3.5×10^{-5}	7.4×10^{-4}
R_{r1}	5.0×10^{-5}	5.8×10^{-4}
R_{rm}	2.2×10^{-5}	6.2×10^{-4}
R_{e}	1.0×10^{-5}	6.2×10^{-4}
R_{m}	2.3×10^{-3}	3.5×10^{-3}
R_1	5.7×10^{-5}	3.8×10^{-3}
R_2	6.8×10^{-6}	6.6×10^{-3}
R_3	1.0×10^{-4}	1.2×10^{-2}
R_4	7.0×10^{-6}	2.3×10^{-2}
R_5	7.3×10^{-5}	4.6×10^{-2}

Table 2. Computed relative errors as defined by Eq. (9), between $\check{R}_{\mathrm{Re}}(x,y)$ and $\check{R}_j(x,y)$.

	Rel Err
R_{r6}	8.4×10^{-6}
R_{r5}	6.7×10^{-3}
R_{r4}	5.4×10^{-3}
R_{r3}	4.5×10^{-3}
R_{r2}	3.7×10^{-2}
R_{r1}	3.1×10^{-3}
R_{rm}	2.4×10^{-3}
R_{m}	8.4×10^{-3}
R_1	7.8×10^{-3}
R_2	8.2×10^{-3}
R_3	1.1×10^{-2}
R_4	1.4×10^{-2}
R_5	1.5×10^{-2}

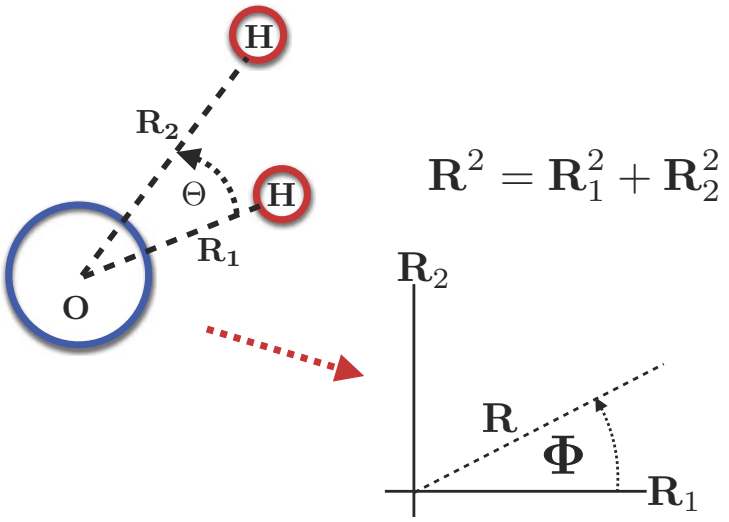

$$\mathbf{R}^2 = \mathbf{R}_1^2 + \mathbf{R}_2^2$$

Figure 1. Coordinate system used for the H_2O PES. Planar slices are taken by fixing values for Θ and Φ.

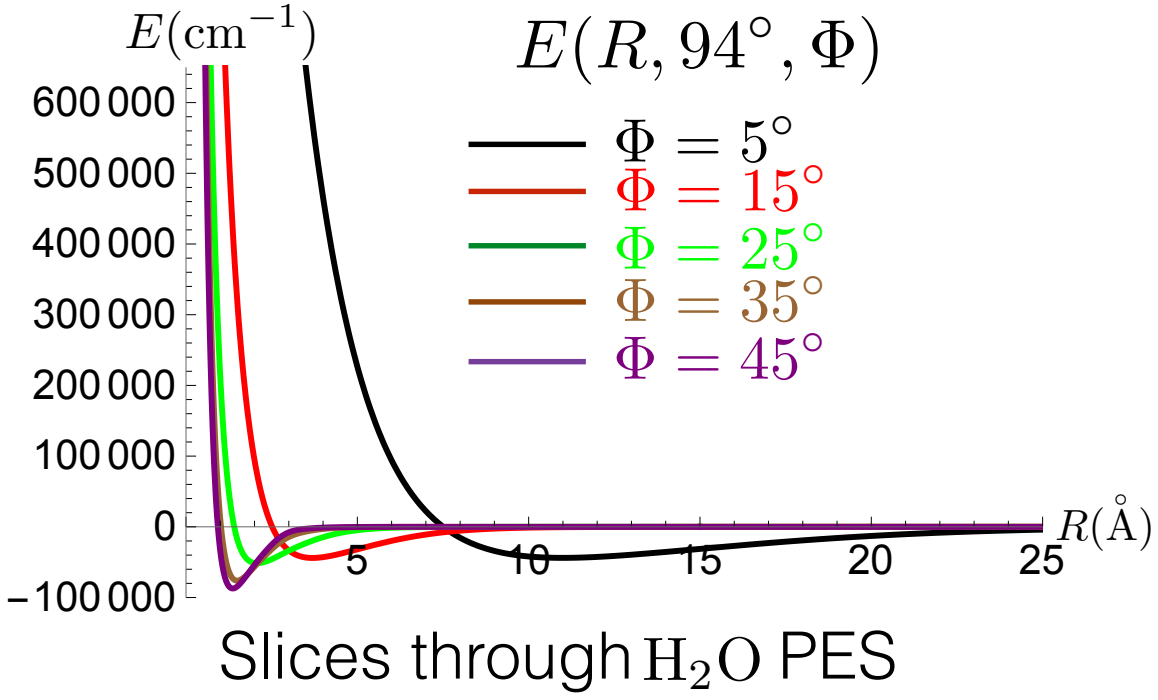

Figure 2. 1-dimensional planar slices curves of $E(R;\Theta{=}94°,\Phi)$.

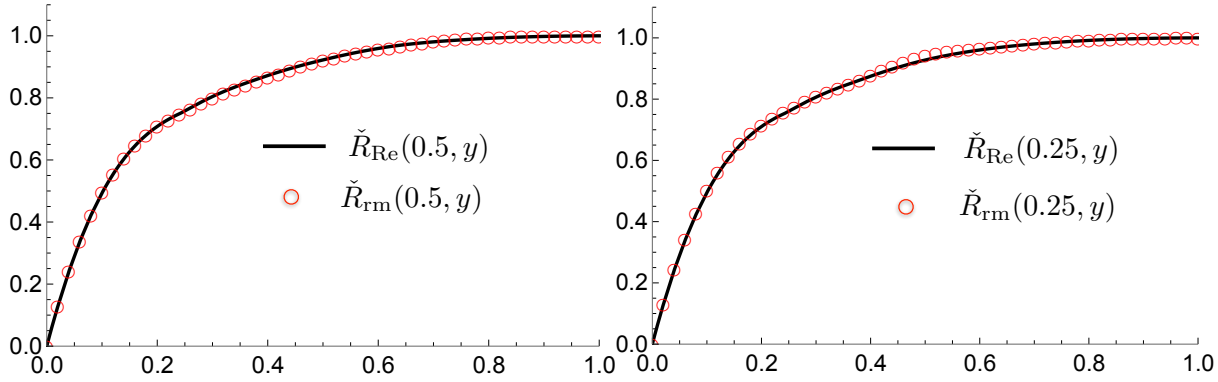

Figure 3. The left graph compares the canonical functions $\check{R}_{\mathrm{Re}}(0.5, y)$ (solid black curve) and $\check{R}_{\mathrm{rm}}(0.5, y)$ (red circles), while the right graph compares $\check{R}_{\mathrm{Re}}(0.25, y)$ and $\check{R}_{\mathrm{rm}}(0.25, y)$.

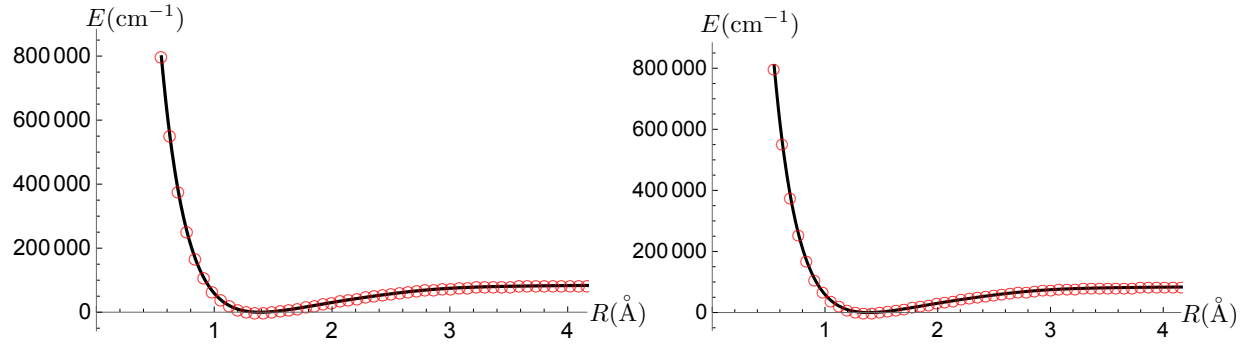

Figure 4. The left graph shows the true potential slice $E(R, 100°, 40°)$ (solid black curve) vs. the approximation $\hat{E}(R, 100°, 40°)$ (red circles) while the right graph shows the true potential vs. the approximation $\tilde{E}(R, 100°, 40°)$.

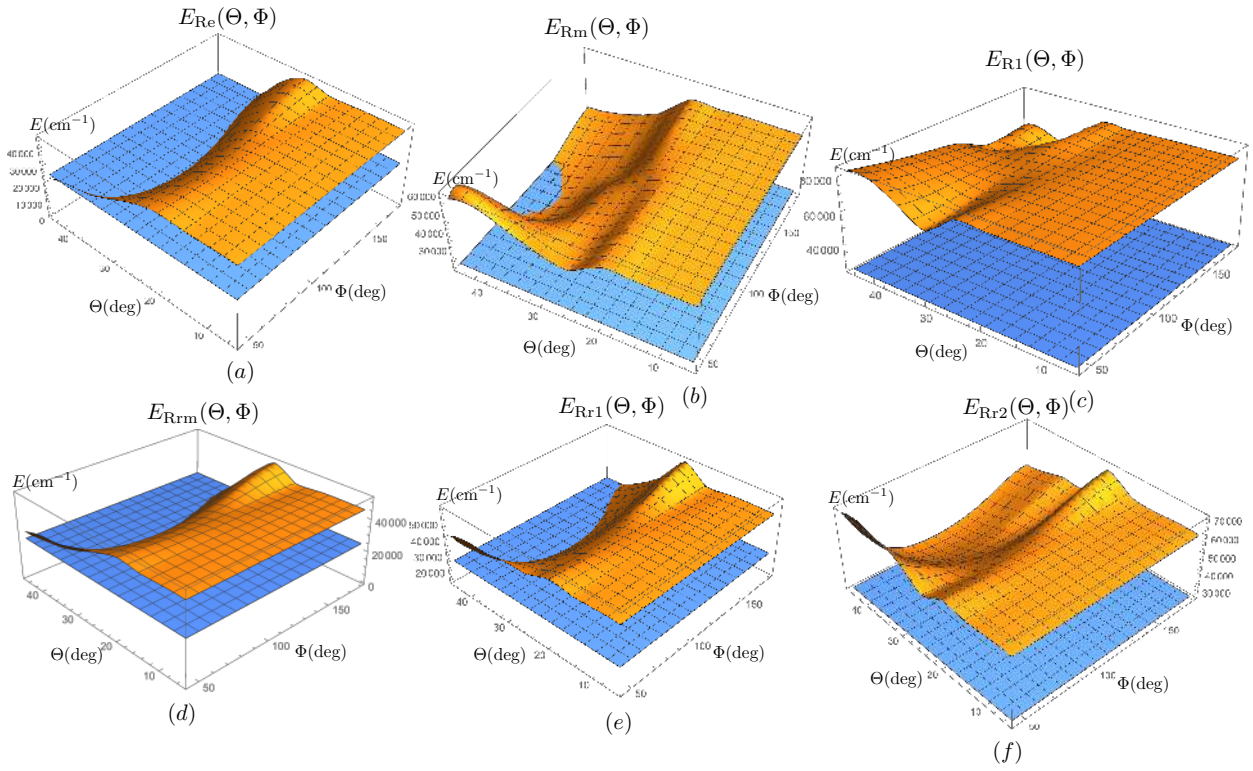

Figure 5. Energy surfaces as functions of the angular variables (Θ,Φ) indicating the portions that lie above and below the 25,000.0 cm^{-1} level (planar surface).

References

(1) Born, M.; Oppenheimer, R. Zur Quantentheorie der Molekeln. *Ann. Phys*. **1927**, *389*, 457-484.

(2) Murrell, J. N.; Carter, S.; Farantos, S. C.; Huxley, P.; Varandas, A. J. C. *Molecular Potential Energy Functions*; John Wiley & Sons: Chichester, U.K., 1984.

(3) Ball, P. Beyond the Bond. *Nature* **2011**, *469*, 26-28.

(4) Bytautas, L.; Bowman, J. M.; Huang, X.; Varandas, A. J. C. Accurate Potential Energy Surfaces and Beyond: Chemical Reactivity, Binding, Long-Range Interactions, and Spectroscopy. *Adv. Phys. Chem*. **2012**, *2012*, 679869.

(5) Stone, A. J. *The Theory of Intermolecular Forces*, 2nd ed.; Oxford University Press: Oxford, U.K., 2013.

(6) Schatz, G. C. The Analytical Representation of Electronic Potential-Energy Surfaces. *Rev. Mod. Phys.* **1989**, *61*, 669-688.

(7) Hollebeek, T.; Ho, T.-S.; Rabitz, H. Constructing Multidimensional Molecular Potential Energy Surfaces from ab Initio Data. *Annu. Rev. Phys. Chem.* **1999**, *50*, 537-570.

(8) Collins, M. A. Molecular Potential-Energy Surfaces for Chemical Reaction Dynamics. *Theor. Chem. Acc.* **2002**, *108*, 313-324.

(9) Dawes, R.; Thompson, D. L.; Wagner, A. F.; Minkoff, M. Interpolating Moving Least-Squares Methods for Fitting Potential Energy Surfaces: A Strategy for Efficient Automatic Data Point Placement in High Dimensions. *J. Chem. Phys.* **2008**, *128*, 084107.

(10) Dawes, R.; Thompson, D. L.; Wagner, A. F.; Minkoff, M. Ab Initio Wavenumber Accurate Spectroscopy: $^{1}CH_2$ and HCN Vibrational Levels on Automatically Generated IMLS Potential Energy Surfaces. *J. Phys. Chem. A* **2009**, *113*, 4709-4721.

(11) Braams, B. J.; Bowman, J. M. Permutationally Invariant Potential Energy Surfaces in High Dimensionality. *Int. Rev. Phys. Chem.* **2009**, *28*, 577-606.

(12) Handley, C. M.; Popelier, P. L. A. Potential Energy Surfaces Fitted by Artificial Neural Networks. *J. Phys. Chem. A* **2010**, *114*, 3371-3383.

(13) Behler, J. Neural Network Potential-Energy Surfaces in Chemistry: A Tool for Large-Scale Simulations. *Phys. Chem. Chem. Phys*. **2011**, *13*, 17930-17955.

(14) Jiang, B.; Li, J.; Guo, H. Potential Energy Surfaces from High Fidelity Fitting of ab Initio Points: The Permutation Invariant Polynomial – Neural Network Approach. *Int. Rev. Phys. Chem.* **2016**, *35*, 479-506.

(15) Majumder, M.; Ndengue, S. A.; Dawes, R. Automated Construction of Potential Energy Surfaces. Mol. Phys. **2016**, *114*, 1-18.

(16) Metz, P. M.; Piszczatowski, K.; Szalewicz, K. Automatic Generation of Intermolecular Potential Energy Surfaces. *J. Chem. Theory Comput.* **2016**, *12*, 5895-5919.

(17) Lucchese, R. R.; Rosales, C. K.; Rivera-Rivera, L. A.; McElmurry, B. A.; Bevan, J. W.; Walton, J. R. A Unified Perspective on the Nature of Bonding in Pairwise Interatomic Interactions. *J. Phys. Chem. A* **2014**, *118*, 6287-6298. In this reference, the notation $V(R)$ corresponds to the notation $E(R)$ used in the current work.

(18) Walton, J. R.; Rivera-Rivera, L. A.; Lucchese, R. R.; Bevan, J. W. A General Transformation to Canonical Form for Potentials in Pairwise Interatomic Interactions. *Phys. Chem. Chem. Phys*. **2015**, *17*, 14805-14810.

(19) Walton, J. R.; Rivera-Rivera, L. A.; Lucchese, R. R.; Bevan, J. W. Canonical Potentials and Spectra within the Born-Oppenheimer Approximation. *J. Phys. Chem. A* **2015**, *119*, 6753-6758. In this reference, the notation $V(R)$ corresponds to the notation $E(R)$ used in the current work.

(20) Walton, J. R.; Rivera-Rivera, L. A.; Lucchese, R. R.; Bevan, J. W. From H_2^+ to the Multidimensional Potential of the Intermolecular Interaction Ar·HBr: A Canonical Approach. *Chem. Phys. Lett*. **2015**, *639*, 63-66.

(21) Walton, J. R.; Rivera-Rivera, L. A.; Lucchese, R. R.; Bevan, J. W. A Canonical Approach to Multi-Dimensional van der Waals, Hydrogen-Bonded, and Halogen-Bonded Potentials. *Chem. Phys*. **2016**, *469-470*, 60-64.

(22) Walton, J. R.; Rivera-Rivera, L. A.; Lucchese, R. R.; Bevan, J. W. Canonical Approaches to Applications of the Virial Theorem. *J. Phys. Chem. A* **2016**, *120*, 817-823.

(23) Walton, J. R.; Rivera-Rivera, L. A.; Lucchese, R. R.; Bevan, J. W. A Canonical Approach to Forces in Molecules. *Chem. Phys*. **2016**, *474*, 52-58.

(24) Walton, J. R.; Rivera-Rivera, L. A.; Lucchese, R. R.; Bevan, J. W. Canonical Force Distributions in Pairwise Interatomic Interactions from the Perspective of the Hellmann-Feynman Theorem. *J. Phys. Chem. A* **2016**, *120*, 3718-3725.

(25) Walton, J. R.; Rivera-Rivera, L. A.; Lucchese, R. R.; Bevan, J. W. Morse, Lennard-Jones, and Kratzer potentials: A Canonical Perspective with Applications. *J. Phys. Chem. A* **2016**, *120*, 8347-8359.

(26) Walton, J. R.; Rivera-Rivera, L. A.; Lucchese, R. R.; Bevan, J. W. Is There any Fundamental Difference Between Ionic, Covalent, and Others Types of Bond? A Canonical Perspective on the Question. *Phys. Chem. Chem. Phys*. **2017**, *19*, 15864-15869.

(27) Polyansky, O. L.; Ovsyannikov, R. I.; Kyuberis, A. A.; Lodi, L.; Tennyson, J.; Zobov, N. F.

Calculation of Rotation-Vibration Energy Levels of the Water Molecule with Near-Experimental Accuracy Based on an ab Initio Potential Energy Surface. *J. Phys. Chem. A*, **2013**, *117*, 9633-9643.